

Update of Wave Statistics Standards for Classification Rules*¹

Håvard Nordtveit AUSTEFJORD*, Guillaume de HAUTECLOCQUE**, Michael JOHNSON***, Tingyao ZHU****

1. INTRODUCTION

The world's commercial shipping in global service is designed to structurally withstand a severe wave environment defined by the International Association of Classification Societies (IACS) - namely IACS "Rec. No. 34 rev1" (2001), which provides details of the North Atlantic Ocean, principally in the form of a scatter diagram giving the occurrence statistics of combinations of significant wave height (H_s) and average zero up-crossing wave period (T_z).

IACS has faced some criticism of Rec. No. 34 rev1 (2001) because the underlying statistical data originates in historical 'eyeball' observations from ships. Whilst these data were the best available at the time, studies have shown inaccuracies in human estimates. The effect of weather avoidance is embedded in the data but unquantifiable, and any bias, for example due to fixed shipping routes or ship types, cannot be identified either. Furthermore, the last observations included date back to 1984, so there is also concern that long term changes since that time are missing.

In recent years numerical wave modelling has improved greatly in quality and has also become more readily available to the engineering community. Furthermore, the International Maritime Organization (IMO) has made the public broadcast of ship positions (Automatic Identification System, AIS) mandatory; this was intended as an aid to navigation local to any particular ship, but the aggregation of such records globally has provided an enormously valuable dataset. These two developments led IACS to propose a project team in 2018 to consider updating Rec. No. 34, with the idea that the AIS tracking data could be combined with co-located wave model data for the North Atlantic to produce an unbiased wave scatter diagram. The project team has submitted its work to IACS "Rec. No. 34 rev2"; this paper makes public much of the technical work performed in order to establish this updated recommendation.

In this paper, the geographical area of review and the sources of ship track and wave model data are first presented. The method to calculate a 'raw' scatter diagram is given, together with work underlying the recommendation for spectra shape and spreading. This is followed by a description of a smoothing process employed to sanitise the raw scatter diagram. Results are then presented, showing how, for a testing database of 70 different ship types, ship responses (ship motion, accelerations, and wave loads) are expected to change when comparing the new "Rec. No. 34 rev2" with the old "Rec. No. 34 rev1 (2001)". Finally, known limitations of the approach are identified and discussed.

2. DATA SOURCE

2.1 Wave Hindcast

The sources underlying the Rec. No. 34 rev1 scatter-diagram are visual observations from ships, last published in 1986¹. Whilst some corrections were applied, those visual observations have been reported to have limited accuracy, especially concerning wave period². Since Rec. No. 34 rev1, significant progress has taken place. Numerical hindcast analyses are nowadays common practice, and several reliable global datasets are publicly available. Based on the analysis of different datasets³, the IOWAGA (Integrated Ocean Waves for Geophysical and other Applications) dataset from Ifremer (Institut Français de Recherche pour l'Exploitation de la Mer) is used in this work⁴. As the IOWAGA dataset does not store full spectra, it is complemented with ERA5 (ECMWF Reanalysis v5) dataset⁵ from ECMWF (European Centre for Medium-Range Weather

*¹ This paper has been originally published in the Proceedings of 9th International Conference on Marine Structures. The permission to reproduce this paper in this Journal has been obtained from the Technical Programme Committee of the conference.

* Det Norske Veritas, Oslo, Norway

** Bureau Veritas, Paris, France

*** Lloyds Register, Southampton, UK

**** Nippon Kaiji Kyokai (ClassNK), Tokyo, Japan

Forecasts) in section 5.

2.2 Ship Position

As Rec. No. 34 is supposed to reflect waves encountered by ships, it is important to consider realistic combinations of routes and wave data^{6) 7) 8)}. The best way to do this is to combine millions of in-voyage locations with individually co-located wave data. This naturally gives a full representation of the routing effect in a ‘routed’ scatter-diagram. Voyages of over twenty thousand vessels were established by cleaning and resampling AIS data to the same temporal resolution as the hindcast wave data.

The fleet is limited to cargo and passenger vessels longer than 90m. This means most commercial seagoing ships are included. Excluded are many fishing vessels, offshore vessels, naval ships, and ships operating at fixed locations e.g. FPSOs.

The time period analysed ranged from 2013 to 2020 (seven full years). The collection of voyages was made in the North-Atlantic, as defined by Fig. 1. The choice of this area is further discussed in section 7. Coastal traffic near islands was discarded (~50 nautical miles).

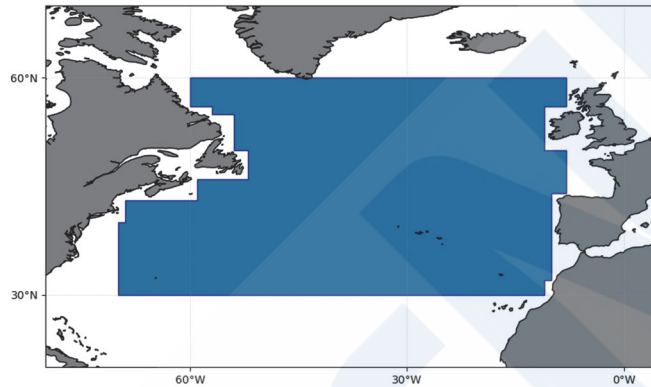


Fig. 1 Definition of North-Atlantic area for this work.

2.3 Database of Ship Responses

The final objective of the new wave statistics standard is a better long-term prediction of ship responses. It is thus important to have this in mind when evaluating the different assumptions and compromises made on the way to this new wave standard. To tackle this, a database of 3D linear seakeeping responses was used.

The vessels included are presented in Table 1. For each vessel, 3D BEM linear calculation⁹⁾ is performed. The transfer functions are output for the quantities listed in Table 2. The RAOs are calculated with a 5° heading resolution, and are available at four speeds: 0 knots, 5 knots, Froude number of 0.1 and 75% of the service speed.

Table 1 Ship database, number of ships investigated for each type and loading condition.

Ship type	Full	Ballast
Tanker	16	11
Bulk and Cargo	19	16
Container-vessel	21	10
LNG	5	0
LPG	5	0
RoRo	3	0
Passenger-ship	5	0
Total	74	37

Furthermore, for each response, a characteristic period T_c is calculated thanks to the available regression in¹⁰⁾; the characteristic length L/α from¹⁰⁾ is converted to period: $T_c^2 = (2 * \pi * L) / (g * \alpha)$. Note that in this work, the characteristic period is not used for any quantitative derivation; but only to display results in a scale allowing for physical interpretation.

Fig. 2 and Fig. 3 illustrate this responses dataset, showing two RAOs, with very different characteristic periods: the vertical

bending moment of a long ship with large T_c , and the horizontal bending moment of a short ship (low T_c).

Table 2 Type of ship responses included in the dataset.

RAO label	Description
VBM	Vertical Bending Moment amidship
HBM	Horizontal Bending Moment amidship
VSF	Vertical Shear Force, aft quarter
Pitch	Pitch motion
Acc. Surge	Surge acceleration
Acc. Sway	Sway acceleration
Pressure wl	Waterline pressure amidship
Roll	Roll motion

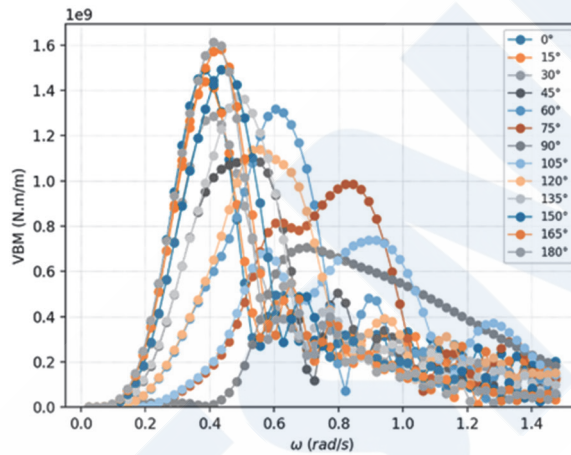


Fig. 2 VBM RAOs, long ship, $L = 370\text{m}$, $T_c = 18\text{s}$.

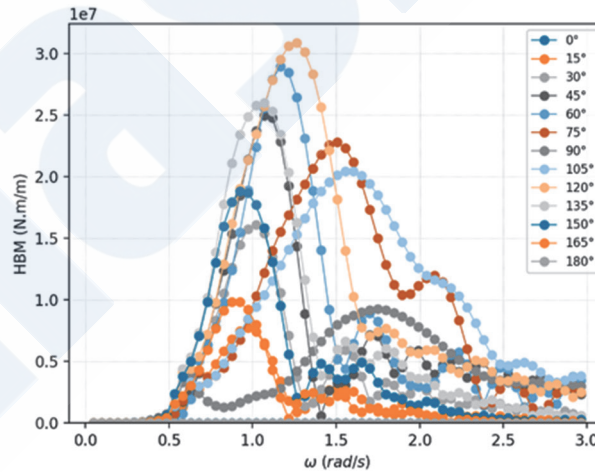


Fig. 3 HBM RAOs short ship, $L = 90\text{m}$, $T_c = 6\text{s}$.

3. DISCRETE SCATTER-DIAGRAM

The approach for deriving discrete scatter diagrams with bad weather avoidance is summarised as follows:

- Download AIS and IOWAGA hindcast data within the North-Atlantic area for a period of 7 years (from June 1st 2013 to June 30th 2020).
- Clean and resample AIS data to 3-hour resolution, including outlier removal and interpolation to fill gaps in the records. Match each AIS data point to the nearest hindcast data point.

- Place encountered significant wave heights H_s and mean wave periods (T_{0m1}) in 0.1m and 0.1s bins. Here, $T_{0m1}(= 2\pi(m_{-1}/m_0))$ is a mean wave period (s), where m_n is the spectral moment of order n.

4. STATISTICAL MODEL

The previous section introduced the process followed by the IACS working group to derive the Rec. No. 34 rev2 scatter-diagram from the combination of vessel tracks and hindcast wave data.

The empirical scatter-diagram obtained from AIS and hindcast data is fitted with a statistical model. It smooths out some of the sampling uncertainties, allows the possibility to extrapolate to unobserved wave periods and provides the scatter-diagram in a compact form (the scatter-diagram can be reconstructed at any desired resolution from a few coefficients).

The statistical model underlying Table 1 of the Rec. No. 34 rev2 is written as:

$$p(H_s, T_{0m1}) = p_H(H_s) * p_{T_{0m1}}(T_{0m1}|H_s) \quad (1)$$

Where $p_H(H_s)$ is the marginal distribution of the significant wave height, and $p_{T_{0m1}}(T_{0m1}|H_s)$ the conditional distribution of the mean wave period.

4.1 Marginal Distribution of H_s

A mixture of Weibull distributions is used to model the marginal distribution. The coefficients (given in Table 3) are determined by MLE (maximum likely-hood estimate) based on the discrete scatter diagram.

$$P_H(H_s) = \chi F_{H,1}(H_s) + (1 - \chi)F_{H,2}(H_s) = 1 - \chi \exp\left[-\left(\frac{H_s - \varepsilon}{\lambda_1}\right)^{\alpha_1}\right] - (1 - \chi) \exp\left[-\left(\frac{H_s - \varepsilon}{\lambda_2}\right)^{\alpha_2}\right] \quad (2)$$

Table 3 Hs distribution coefficients.

	Coefficient
α_1	1.4230
ε	0.9360
λ_1	1.8150
α_2	1.3940
λ_2	2.8050
χ	0.9499

4.2 Conditional Model

The conditional mean wave period distribution is modelled as a split generalized normal distribution:

$$p_{T_{0m1}}(t|H_s) = \begin{cases} c \cdot e^{-\left[\frac{x_0-t}{\sigma_l}\right]^{d_l}} & \text{for } t < x_0 \\ c \cdot e^{-\left[\frac{t-x_0}{\sigma_u}\right]^{d_u}} & \text{for } t \geq x_0 \end{cases} \quad (3)$$

With

$$c = \frac{1}{\sigma_l \Gamma\left(1 + \frac{1}{d_l}\right) + \sigma_u \Gamma\left(1 + \frac{1}{d_u}\right)}$$

The parameters σ_u , σ_l and x_0 are fitted, for each H_s bin, by MLE. The dependency of those parameters with H_s are then fitted with the shapes described in equation (4) using least-square. Table 4 provides the coefficients thus obtained.

$$\begin{aligned}
x_0(h_s) &= l_0 + 1.0 * h_s + l_1 * h_s * \sqrt{h_s} \\
\sigma_u(h_s) &= \begin{cases} su_2 + su_1 * \left(1 - \cos\left(\frac{\pi * h_s}{su_0}\right)\right) * 0.5 & \text{for } h_s < su_0 \\ (su_2 + su_1) * \cos(\sigma_d * \pi) & \text{for } h_s \geq su_0 \end{cases} \\
&\quad \text{with } \sigma_d = \frac{1}{1 + e^{-su_3 * (h_s - su_0)}} - 0.5 \\
\sigma_l(h_s) &= sl_0 * h_s + sl_1 \\
d_u &= 2 \\
d_l &= 3
\end{aligned} \tag{4}$$

Table 4 Coefficients for conditional model.

	Coefficient
l_0	5.427251
l_1	-0.085340
su_0	2.549443
su_1	2.435955
su_2	0.705177
su_3	0.133225
sl_0	0.018557
sl_1	1.005918

Finally, discretisation is performed into 1m and 1s bins to get the final scatter-diagram. Values in each bin are calculated using midpoints, except for $H_s = [0.0\text{m}, 1.0\text{m}]$ where exact integration is used. The obtained discretized scatter-diagram is given in appendix (Fig. 19).

4.3 Contribution Coefficients

Using the newly defined scatter-diagram, and working with the ship database introduced in 2.3, contribution coefficients can be calculated to show the sensitivity to the seas state of both extreme and fatigue loads. The knowledge of those contribution coefficients allows prioritisation of the relevant sea-states when simplified assessments are needed.

The contribution coefficients are calculated using the response dataset from section 2.3, assuming a JONSWAP spectrum with $\gamma = 1.5$ and a directional spreading of \cos^3 .

From Fig. 4, the H_s of the sea-states contributing the most to the extreme are, roughly speaking, between, 7.5m and 16.5m. The characteristic period largely explains the variations observed: small T_C are associated with small H_s , large T_C with large H_s . As a simplification, hereafter, sea-states with $H_s > 10\text{m}$ are considered as extreme sea-states.

The range of sea-states contributing to the fatigue damage are, on the other hand, lower; in the range [3m, 7m] (Fig. 5).

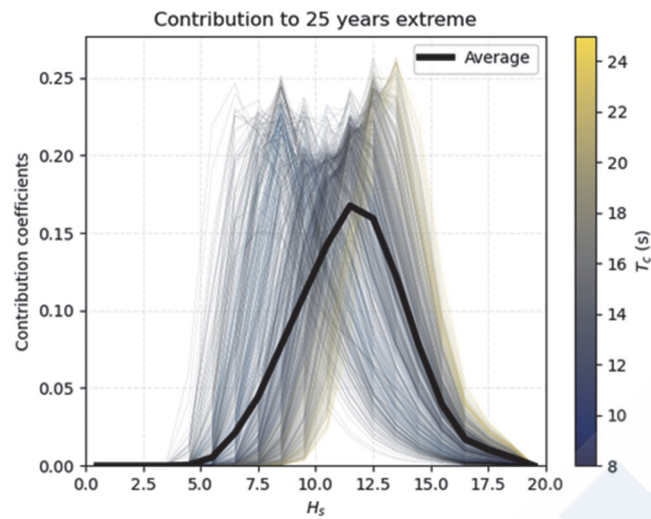


Fig. 4 Contribution coefficients for extreme.

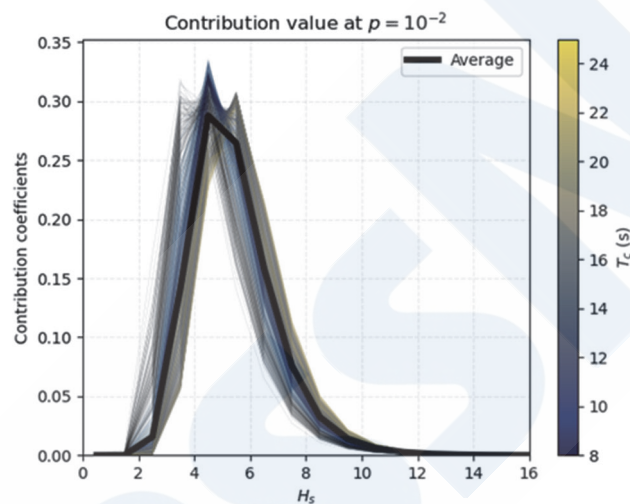


Fig. 5 Contribution coefficients for fatigue loads.

5. SPECTRUM SHAPE

In Rec. No. 34 rev1, the spectral shape is a two parameters Pierson-Moskowitz spectrum (equivalent to JONSWAP with $\gamma = 1.0$), associated with \cos^2 spreading. In the present studies, analysis of full directional spectra from hindcast data has shown that JONSWAP spectrum with $\gamma = 1.5$ and a \cos^3 spreading was more appropriate to represent extreme sea-states. Furthermore, this spectral shape provides accurate results for fatigue loads as well. This section gives some background justifications.

The full spectra data here analysed are from the model ERA5, at a single point located in the North Atlantic, over the period of 25 years (1990-2014).

Fig. 6 shows the shape of 306 sea-state spectra contributing the most to the 25-years extreme ($\sim H_s > 10\text{m}$), normalised according to T_{0m1} . The extreme sea states have remarkably constant shape and seem to be well represented by a JONSWAP spectrum with peakedness factor $\gamma = 1.5$. This value of 1.5 has been obtained by a least-square minimisation. It is also observed that matching T_{0m1} or T_p provides much better results than $T_Z^{(1)}$.

A slight trend of gamma increasing with H_s was observed; however, it was found that setting gamma as a function of H_s did not significantly improve the overall accuracy of ship responses. For simplicity and practicality, a fixed value $\gamma = 1.5$ is then recommended.

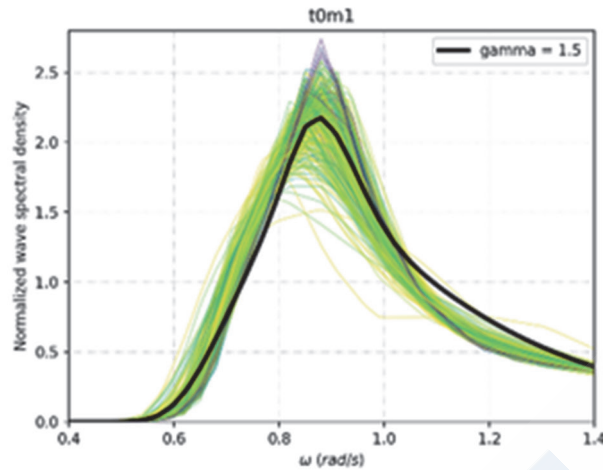


Fig. 6 Shapes of contributing spectra ($H_s > 10\text{m}$) and the chosen parameterized spectrum (JONSWAP, $\gamma = 1.5$), based on 25 years of hindcast data.

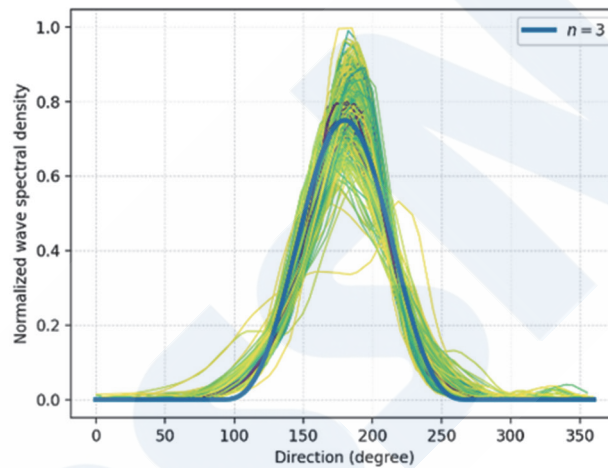


Fig. 7 Shapes of contributing spectra ($H_s > 10\text{m}$) as function of headings, together with the parametrized shape (\cos^3).

Similarly, Fig. 7 shows the directional shape of sea-states contributing to the extreme. As with the frequency shape, the directional spreading is very similar among the different sea-states and well approximated by a \cos^n formulation with $n=3$.

Finally, to evaluate the accuracy loss induced by this simple parametrization, a validation is performed with the ship RAO dataset introduced section 2.3 and the ERA5 directional wave dataset introduced earlier in this section. The 25 years extreme values are calculated for all ship responses:

- Using full spectra (reference)
- Using $\gamma = 1.0$ and $n = 2$ (Rec. No. 34 rev1)
- Using $\gamma = 1.5$ and $n = 3$ (Rec. No. 34 rev2)

For extreme loads, the Rec. No. 34 rev1 shape results in a 7% quadratic error compared with the benchmark full spectrum case, which is reduced to 5% using Rec. No. 34 rev2 parameters.

Fatigue loads (at 10^{-2} probability as the reference value) are less sensitive to spectrum shape. With the same testing data set, Rec. No. 34 rev1 and Rec. No. 34 rev2 show a quadratic error of 2.7% and 3.2% compared with the benchmark case, respectively. Those errors are considered comparable and acceptable.

These findings are confirmed by a similar analysis conducted at several locations¹¹⁾.

6. OPERATIONAL PROFILE

The Rec. No. 34 rev1 includes recommendations for how ships are assumed to operate in different sea conditions. Equal probability for all ship headings is specified, and zero speed is assumed when evaluating extreme wave loads (strength assessment).

In this section, using results from the combined AIS-hindcast dataset described in Section 2, the probability distributions of ship speeds and relative wave headings are estimated. All types of merchant ships over 90m navigating in the North Atlantic Area shown in Fig. 1 are considered.

The correlation between speed and heading with significant wave height is complex. In the following, it is assumed that the speed and heading can be investigated separately.

6.1 Heading

Accounting for the AIS-IOWAGA data including the entire range of H_s , we observe that the heading profile is equiprobable, as currently assumed in Rec No. 34 rev1 (Fig. 8). Uniform distribution is thus perfectly suited to fatigue calculations.

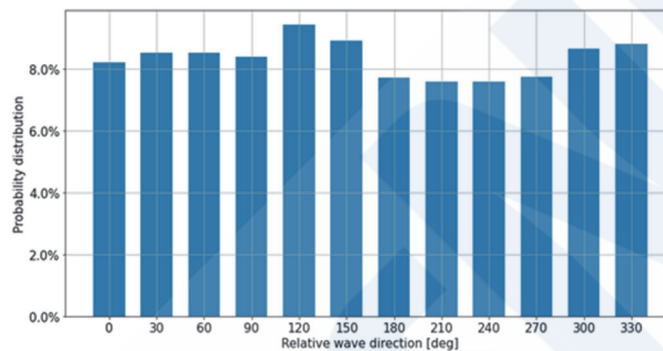


Fig. 8 Heading histogram, all data.

However, looking only at extreme sea-states, the picture is different: beam seas are less likely, as shown in Fig. 9. This figure presents the data in North-Atlantic only; it has been checked that using world-wide data which provides a similar picture. Two factors can explain this observation:

- Ship's captains avoid beam seas in harsh weather, to limit roll motion and increase stability.
- Harsh weather happens in locations where routes are mostly east-west, with dominant wave direction from west.

While the first explanation is considered as the main one, the below data cannot distinguish between the two effects. Whatever the cause, the practical effects are the same and evaluated on the ship response database.

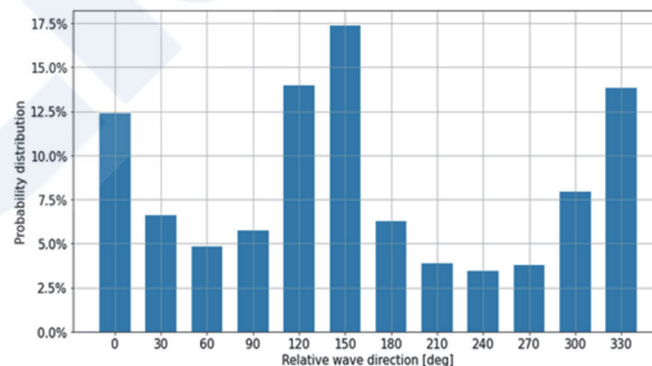


Fig. 9 Heading histogram, $H_s > 10m$.

Fig. 10 shows the relative differences between extreme responses considering the headings equiprobable, or with the same distribution as Fig. 9. A constant speed 5 knots has been assumed for simplicity. The effect is small, and keeping a constant probability for headings thus appears to be a good compromise between simplicity and accuracy.

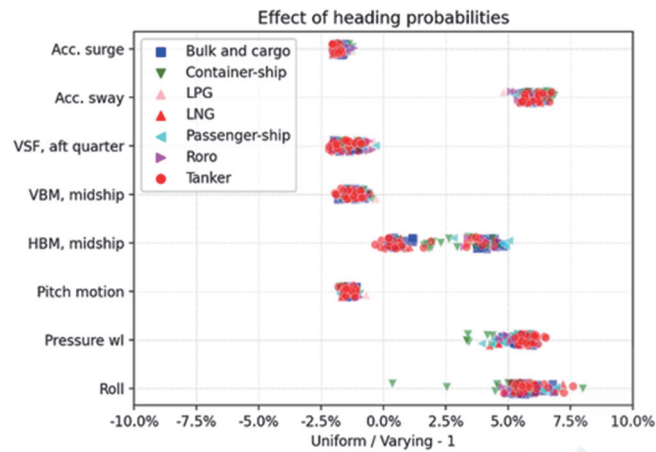


Fig. 10 Response sensitivity to heading distribution.

6.2 Speed

In the same fashion, the relationship between ship speed and heading is investigated. From Fig. 11 it is observed that speed in head seas reduces significantly with wave-height. The two most plausible reasons are:

- Voluntary speed reduction to limit ship motions.
- Involuntary speed reduction due to added resistance in waves.

Looking slightly deeper, it appears that the speed reduction is strongly dependent on the relative wave heading. Fig. 12 shows the speed reduction for each heading. It appears that the reduction is larger in head sea than in following sea.

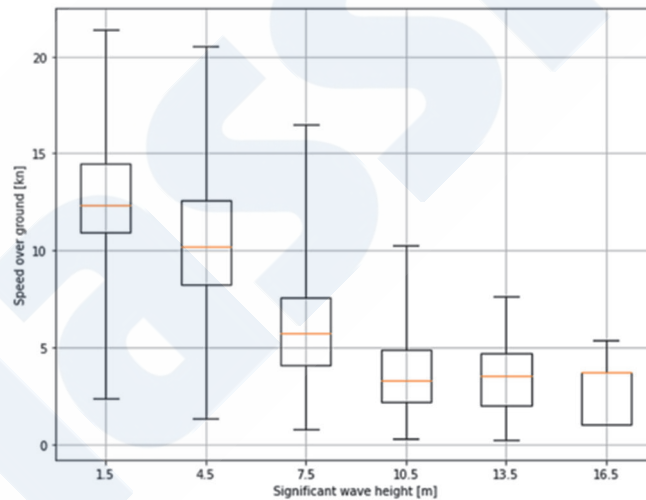


Fig. 11 Speed versus wave height in head sea, all ships.

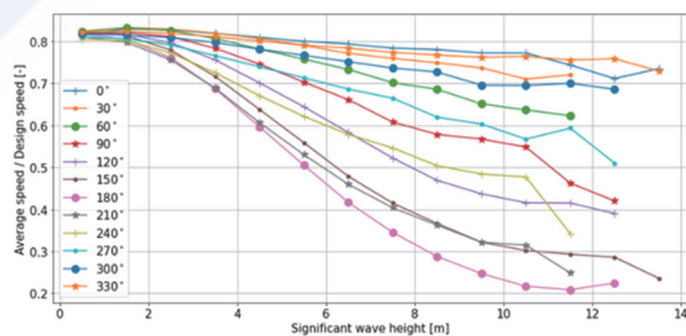


Fig. 12 Average ship speed as function of H_s and relative wave heading, 0 being following sea and 180 head sea.

To assess the sensitivity of long-term results to assumptions made on vessel speed, long-term calculations of extreme responses are performed using data from Fig. 12, simplified as follows to be compatible with the RAO dataset:

- 0.75 Vs for 0°, 30° and 330°.
- Froude number = 0.1 for 60°, 90°, 270° and 300°.
- 5 knots for 120°, 150°, 180°, 210° and 240°.

The results are then compared with the less refined assumption from the Common Structural Rules for bulk carriers and oil tankers¹²⁾: fixed 5 knots. The headings are considered equiprobable in both cases.

From Fig. 13, it is observed that assuming a 5 knots speed for extreme has small effect on most of the responses. However, large difference may arise for roll motion and related quantities such as pressure on waterline. This is linked to the roll motion which can be large for low GM vessels in stern-quartering seas at high speed¹³⁾. While this is relevant, the discrepancies are overestimated in our calculations, for three reasons:

- The GMs used in the ship response dataset are a lower bound (full, scantling GM). However, ships tend to operate on average at larger GM.
- In the ship response dataset, the roll damping is linear (6%) and does not vary with speed. In reality, lift damping as well as the quadratic effect would attenuate large roll angles at large speed.
- The fact that large roll angles are likely for low GM vessels in stern quartering seas is known and operational guidance are given to avoid those conditions¹³⁾. The speed/heading/ H_s statistics observed from AIS and hindcast do not include GM data, and do not allow this to be accounted for.

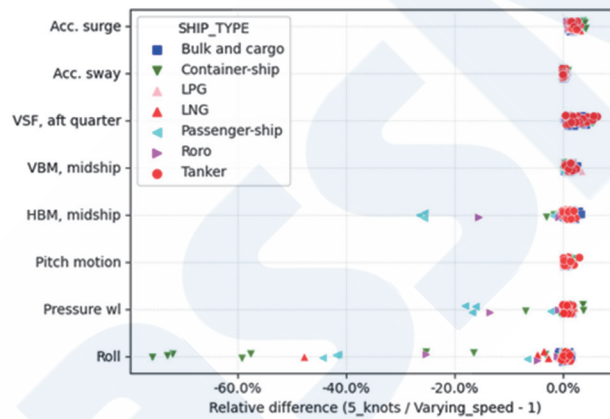


Fig. 13 Effect of fixed 5 knots assumption.

Filtering out ships having low GM with much larger roll motion at forward speed, we obtain Fig. 14, which shows that the 5 knots assumption is acceptable.

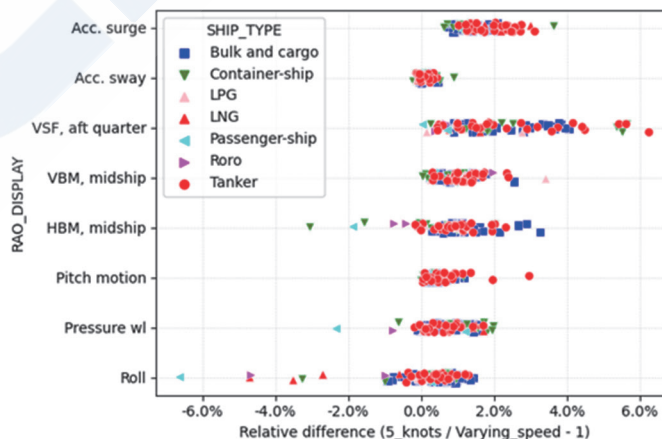


Fig. 14 Effect removing ship with high stern quartering roll.

For vessels with low metacentric height and operating without reduced speed in stern quartering seas appropriate speed and viscous damping need to be applied when evaluating roll related responses by numerical simulations. Furthermore, it is assumed that these effects can be considered in the development of rule formulae of roll motions by individual classification society.

6.3 Summary on Operational Profile

The uniform heading distribution currently used in the IACS Common Structural Rules for bulk carriers and oil tankers (CSR) and in Rec. No. 34 rev1 is thus confirmed and the continued use is justified in Rec. No. 34 rev2.

Using 5 knots for vertical shear force and bending moment and for loads in general for oil tankers and bulk carriers covered by CSR rules is mostly conservative. At most 1% non-conservatism is observed for roll motion of bulk carriers and tankers. It is therefore considered acceptable to use 5 knots as basis for vertical shear and bending in unified requirements S11 and S11A as well as loads in general for the CSR rules.

7. GEOGRAPHICAL AREA AND LOAD LEVEL

IACS Rec. No. 34 is based on wave data obtained from North Atlantic trade as this represents the most severe area ships tend to operate in. The basic idea of using a harsh design wave environment is that ships should not need to have geographical limitations on their operation.

Deciding on the exact polygon defining the North Atlantic is a subject for discussion. The wave characteristics are not uniform across the whole basin. Selecting a small area with harsher weather will result in a stricter scatter diagram than if the polygon is expanded to include less severe areas. To understand the consequence of the area selection an assessment of wave load level is made.

Hydrodynamic strip theory analyses were performed for 1500 vessels of different ship types and sizes. Each vessel was evaluated at multiple speeds between zero and full forward speed for relative wave directions with 30 degrees spacing.

AIS data for the world fleet is, in this study, limited to merchant vessels longer than 90 meters with a minimum of one year of data. The resulting 44000 vessels are matched with the closest hydrodynamic model in terms of vessel type, length, breadth and service speed. By matching the AIS data with IOWAGA hindcast data each vessel has a known series of wave height, period, relative direction and speed. This is used in long term response evaluation of the midship vertical bending moment at 1 year return period as well as the 10^{-2} exceedance probability.

Fig. 15 presents the ratio between 1-year moment from actual operation normalised by the 25-year design moment obtained using the Rec. No. 34 rev2. Fig. 16 shows the ratio of 10^{-2} moment between experienced and design load used for fatigue assessment in the IACS Common Structural Rules for bulk carriers and oil tankers (CSR).

Two variants of geographical areas are evaluated, one being somewhat smaller than the one finally selected. The smaller harsher area would slightly increase the 25-year extreme design wave loads, resulting in fewer vessels exceeding the 25-year design point. For fatigue the smaller area would easily result in no vessels exceeding the design value, meaning an over conservatism on fatigue loads. The effect of including the highly trafficked Bay of Biscay was considered but found not to make any difference to the loads, typically less than +/- 0.3% on extreme loads.

It is also observed that the different vessel types do not strictly encounter the same sea-states. The option to provide different scatter-diagrams for different types of vessels was considered and quickly discarded and considered not practical. On the other hand, the knowledge from Fig. 15 and Fig. 16 leaves the door open to further development of partial safety factors that would account for this observation.

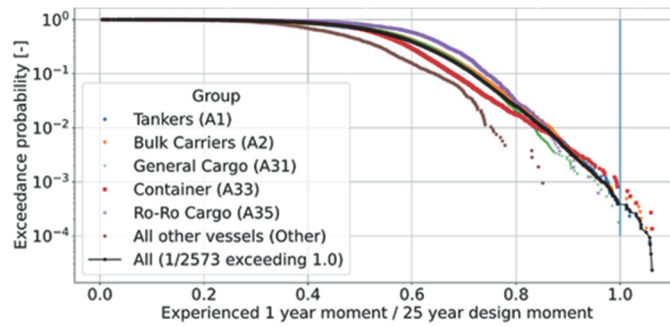


Fig. 15 Exceedance rate of 25-year extreme design moment per year.

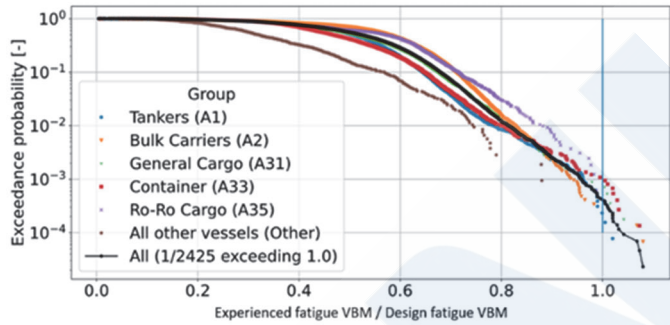


Fig. 16 Exceedance rate of 10^{-2} fatigue design moment.

This study gives an early idea of the level of the design load compared to what the world fleet experiences and may act as input when the final safety level including both load and capacity will be calibrated by IACS.

8. CONSEQUENCE ASSESSMENT

The changes from Rec. No. 34 rev1 to rev2 are summarized in Table 5. The most significant change is the scatter-diagram itself, which induces relative lower loads. Then, the narrower spectrum and sharp spreading tend to slightly increase the loads respectively. Finally, the new definition of extremes (Return period (RP) =25 years, vs $p = 10^{-8}$) introduces a tiny reduction of the loads.

Table 5 Summary of changes.

	Rec. No. 34 rev1	Rec. No. 34 rev2
Scatter-diagram	Visual observation	Hindcast
Spectrum	Pierson-Moskowitz	JONSWAP $\gamma = 1.5$
Spreading	Cos^2	Cos^3
Extreme definition	$p = 10^{-8}$	RP= 25 years
Heading distribution	Uniform	Uniform
Fatigue reference	NA	$p = 10^{-2}$

The combined consequences of those updates are evaluated on the ship response dataset presented in Section 2.3, for extreme, and for fatigue loads.

Fig. 17 shows the consequences of extreme loads for both Rec. No. 34 rev1 and rev2 on all ship responses. Depending on the vessel and response type, the extreme loads are reduced from 10% to 30%. The characteristic period alone explains most of the variation: the reduction is relatively higher for responses with low characteristic period. Hence, for extreme loads, the new recommendation is – relatively – more favorable to short vessels.

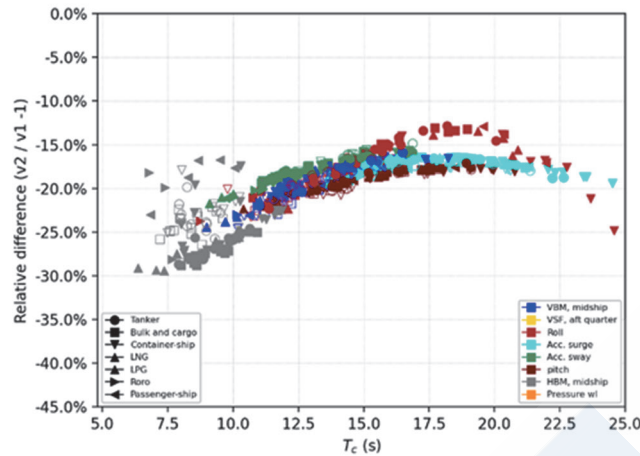


Fig. 17 Consequences on extreme loads.

Fig. 18 shows the consequence of fatigue loads, evaluated at $p = 10^{-2}$ for both Rec. No. 34 rev1 and rev2 on all ship responses. Compared to Rec. No. 34 rev1, the fatigue loads are significantly reduced in average, with reduction from -5% to -50%. As for extreme loads, the characteristic period of the response explains for most of the variation. On the other hand, this time, the Rec. No. 34 rev2 is, relatively, more favorable to long responses (i.e. long vessels).

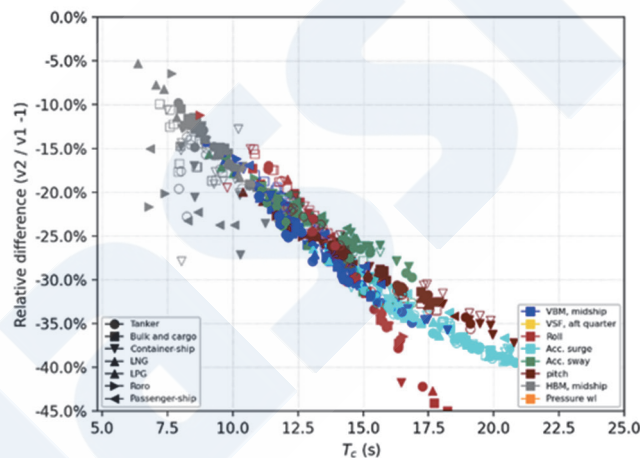


Fig. 18 Consequences on fatigue loads.

9. LIMITATIONS

Whilst the studies, techniques and data used by IACS to contribute to the up-issue of Rec. No. 34 are, at the moment of writing, considered state-of-the-art, there are known limitations. These are highlighted here.

9.1 Wave Models

IACS Rec. No. 34 rev2 relies heavily on numerical hindcast data. Although those have been validated through comparison with buoy data and satellite altimeters some uncertainties remain. Wave modelling is an active academic field and the accuracy of the global wave models is expected to continue to improve year on year.

9.2 Climate Change

The updated wave environment recommendations proposed by IACS are a present day snapshot and do not include any climate forecast change effects. The working group reviewed the work of the Intergovernmental Panel on Climate Change (IPCC), and found that there was a great deal of uncertainty about the effects relevant to shipping. However, even changes at the highest end of IPCC projections of $\pm 0.5\text{m}$ (positive or negative) in extreme wave heights for the North Atlantic would be

expected to have negligible effect on the IACS Rec. No. 34 rev2 scatter diagram due to the robustness of the derivation procedure. Furthermore, ships in service will continue to avoid rough weather at the levels encapsulated in the new scatter diagram. In effect the IACS Rec. No. 34 rev2 scatter diagram does include some future-proofing.

9.3 Bad Weather Avoidance

The bad-weather avoidance embedded within this work represents the current performance level of global shipping. The technical quality, availability and take-up of routing services is increasing under current industry drive towards digitalisation. Therefore, the new recommendation might be regarded as including a slightly conservative bias as time goes on and those improvements become more definite.

9.4 Statistics

Synchronised weather data with ship position was limited to only 7 years. This was compensated by the fact that a huge number of ship positions was used, roughly 4500 ship-years, and that these later years were among the roughest recorded. The amount of data used is considered sufficient to correctly assess the 25 years ship responses, though this limitation is to be kept in mind when using the proposed scatter-diagram to estimate ship response at very low probabilities (i.e. very large return period). Even so, the new scatter diagrams are considered a huge improvement on Rec. No. 34 rev1 derived from eyeball observations.

Finally, the industry standard design approach that uses scatter-diagram is itself an approximation. By grouping time-series data into H_s-T_{0m1} bins, the serial correlation of sea-states is lost and can result in an overestimation bias¹⁴). Up to +5% conservatism on VBM is possible for large vessels.

10. CONCLUSIONS

A new wave standard is defined using state-of-the-art wave data sources combined with a ship position dataset. The wave scatter-diagram is significantly modified and includes the effect of bad-weather avoidance. Furthermore, the spectrum and spreading shapes are slightly narrower than in Rec. No. 34 rev1.

The change of wave loads is not homogenous: it depends on the type of loads and the type and size of the vessels. It thus, theoretically, optimises how the steel is distributed on a vessel, and across the fleet.

While Rec. No. 34 is an important document, it is only one piece acting as input to rule development. The average wave load reduction observed here will not necessarily translate directly into a reduction of the scantling. For instance, the current IACS unified requirement S11A for container vessels considers a routing factor to correct for the fact that Rec. No. 34 rev1 does not account properly for bad weather avoidance; this factor shall thus be adjusted when accounting for Rec. No. 34 rev2.

Further work is thus ongoing within IACS to update downstream documents, such as IACS URS11, IACS URS11A and the Common Structural Rules for bulk carriers and oil tankers¹²).

ACKNOWLEDGMENTS

The work reported here was sponsored by the International Association of Classification Societies. The authors also wish to acknowledge the contributions to this work of Dr. Norio Yamamoto, ClassNK, Quentin Derbanne, Marine Lasbleis, BV, Dr. Eivind Ruth, Dr. Elzbieta Maria Bitner-Gregersen, Dr. Tormod R. Landet, all three of DNV, Dr. Zhenhong Wang, LR.

REFERENCES

- 1) Hogben, N: "Global Wave Statistics", British Maritime Technology, 1986.
- 2) Bitner-Gregersen, EM, Cramer, EH & Korbijn, F: "Environmental Description for Long-Term Load Response of Ship Structures", the Fifth International Offshore and Polar Engineering Conference, 1995.
- 3) de Hauteclocque, G, Zhu, T, Johnson, M, Austefjord, H & Bitner-Gregersen, E: "Assessment of Global Wave Datasets for Long Term Response of Ships", OMAE2020, Volume 2A: Structures, Safety, and Reliability, 2020.
- 4) Arduin, F, Hanafin, J, Quilfen, Y, Chapron, B, Queffeulou, P & Obrebski, M: "Calibration of the IOWAGA Global Wave Hindcast (1991–2011) Using ECMWF and CFSR Winds", *12th International Workshop on Wave Hindcasting and*

Forecasting, Kohala Coast, Hawaii, 2011.

- 5) Hershbach, H, Bell, B, Berrisford, P, Horányi, A, Sabater, JMTN, Nicolas, J, Radu, R, Schepers, D, Simmons, A, Soci, C & Dee, D: “Global Reanalysis: Goodbye ERA-Interim, Hello ERA5”, ECMWF Newsletter No. 159, pp. 17–24, 2019.
- 6) Eisinger, E, Bloch, H & Storhaug, G: “A Method for Describing Ocean Environments for Ship Assessment”, Proc. 6th International Maritime Conference on Design for Safety, Hamburg, 2016.
- 7) Miratsu, R, Fukui, T, Matsumoto, T & Zhu, T: “Quantitative Evaluation of Ship Operational Effect in Actually Encountered Sea States”, 2019. <https://doi.org/10.1115/OMAE2019-95121>.
- 8) Miratsu, R, Fukui, T, Matsumoto, T & Zhu, T: 2020, “Study on Ship Operational Effect for Defining Design Values on Ship Motion and Loads in North Atlantic”, 2020. <https://doi.org/10.1115/OMAE2020-18193>.
- 9) Chen, XB: “Hydrodynamics in Offshore and Naval Applications - Part I”, *Keynote lecture of 6th International Conference on Hydrodynamics*, Perth, Australia, 2004.
- 10) de Hauteclocque, G, Monroy, C, Bigot, F & Derbanne, Q: “New Rules for Container-Ships - Simplified Formulae for Wave Loads.”, the Proceedings of 13th International Symposium on Practical Design of Ships and Other Floating Structures (PRADS2016), Copenhagen, Denmark, 2016.
- 11) de Hauteclocque, G & Lasbleis M: “Extreme Seastate Parametrization and Its Consequences on Ship Responses”, the *Proceedings of 15th International Symposium on Practical Design of Ships and Other Floating Structures (PRADS2022)*, Dubrovnik, Croatia. 2022.
- 12) IACS: “Common Structural Rules for Bulk Carriers and Oil Tankers”, 2014.
- 13) IMO: “Revised Guidance to the Master for Avoiding Dangerous Situations in Adverse Weather and Sea Conditions”, 2007.
- 14) Mackay, E, de Hauteclocque, G, Vanem, E & Jonathan, P: “The Effect of Serial Correlation in Environmental Conditions on Estimates of Extreme Events”, *Ocean Engineering*, Vol 242, 2021.

APPENDIX

		Mean wave period, T_{0m1} (s)															Sum		
		4.5	5.5	6.5	7.5	8.5	9.5	10.5	11.5	12.5	13.5	14.5	15.5	16.5	17.5	18.5		19.5	
Significant wave height, H_s (m)	0.5	6.82	202.00	333.61	187.76	45.59	4.74	0.21	0.00	0.00	0.00	0.00	0.00	0.00	0.00	0.00	0.00	0.00	780.73
	1.5	0.33	2028.35	12750.82	11693.39	7215.76	3006.80	846.07	160.77	20.63	1.79	0.10	0.00	0.00	0.00	0.00	0.00	0.00	37724.81
	2.5	0.00	3.38	2805.81	8517.74	7835.85	5885.37	3608.30	1805.81	737.71	246.00	66.96	14.88	2.70	0.40	0.05	0.00	0.00	31530.96
	3.5	0.00	0.00	23.06	2742.51	4666.81	4100.83	2936.41	1713.38	814.68	315.65	99.66	25.64	5.38	0.92	0.13	0.01	0.00	17445.07
	4.5	0.00	0.00	0.00	82.06	1759.81	2069.19	1715.42	1151.29	625.51	275.12	97.96	28.24	6.59	1.24	0.19	0.02	0.00	7812.64
	5.5	0.00	0.00	0.00	0.08	149.74	811.81	791.81	609.66	375.67	185.26	73.12	23.09	5.84	1.18	0.19	0.02	0.00	3027.47
	6.5	0.00	0.00	0.00	0.00	1.02	147.59	305.37	271.71	190.23	104.79	45.42	15.49	4.16	0.88	0.15	0.02	0.00	1086.83
	7.5	0.00	0.00	0.00	0.00	0.00	4.77	88.62	107.20	86.26	53.35	25.36	9.27	2.60	0.56	0.09	0.01	0.00	378.09
	8.5	0.00	0.00	0.00	0.00	0.00	0.02	9.40	38.70	36.80	25.95	13.63	5.33	1.55	0.34	0.05	0.01	0.00	131.78
	9.5	0.00	0.00	0.00	0.00	0.00	0.00	0.20	9.34	15.15	12.51	7.39	3.12	0.94	0.20	0.03	0.00	0.00	48.88
	10.5	0.00	0.00	0.00	0.00	0.00	0.00	0.00	0.81	5.73	5.96	4.08	1.90	0.60	0.13	0.02	0.00	0.00	19.23
	11.5	0.00	0.00	0.00	0.00	0.00	0.00	0.00	0.02	1.29	2.68	2.23	1.18	0.40	0.08	0.01	0.00	0.00	7.89
	12.5	0.00	0.00	0.00	0.00	0.00	0.00	0.00	0.00	0.11	1.01	1.14	0.72	0.27	0.06	0.01	0.00	0.00	3.32
	13.5	0.00	0.00	0.00	0.00	0.00	0.00	0.00	0.00	0.00	0.22	0.51	0.42	0.18	0.04	0.00	0.00	0.00	1.37
	14.5	0.00	0.00	0.00	0.00	0.00	0.00	0.00	0.00	0.00	0.02	0.19	0.21	0.12	0.03	0.00	0.00	0.00	0.57
	15.5	0.00	0.00	0.00	0.00	0.00	0.00	0.00	0.00	0.00	0.00	0.04	0.09	0.07	0.02	0.00	0.00	0.00	0.22
	16.5	0.00	0.00	0.00	0.00	0.00	0.00	0.00	0.00	0.00	0.00	0.00	0.03	0.04	0.01	0.00	0.00	0.00	0.08
	17.5	0.00	0.00	0.00	0.00	0.00	0.00	0.00	0.00	0.00	0.00	0.00	0.01	0.02	0.01	0.00	0.00	0.00	0.04
	18.5	0.00	0.00	0.00	0.00	0.00	0.00	0.00	0.00	0.00	0.00	0.00	0.00	0.01	0.01	0.00	0.00	0.00	0.02
Sum	7.15	2233.73	15913.30	23223.54	21674.58	16031.12	10301.81	5868.69	2909.77	1230.31	437.79	129.62	31.47	6.11	0.92	0.09	0.00	100000.00	

Fig. 19 Rec. No. 34 rev2 scatter diagram.